



## Copyright Notice

©2004 IEEE. Personal use of this material is permitted. However, permission to reprint/republish this material for advertising or promotional purposes or for creating new collective works for resale or redistribution to servers or lists, or to reuse any copyrighted component of this work in other works must be obtained from the IEEE.

This document was downloaded from Chalmers Publication Library (<http://publications.lib.chalmers.se/>), where it is available in accordance with the IEEE PSPB Operations Manual, amended 19 Nov. 2010, Sec. 8.1.9 (<http://www.ieee.org/documents/opsmanual.pdf>)

(Article begins on next page)

# Frequency Diversity Performance of Coded Multiband-OFDM Systems on IEEE UWB Channels

Matts-Ola Wessman, Arne Svensson, Erik Agrell  
Communication System Group, Department of Signals and Systems,  
Chalmers University of Technology, SE-412 96 Gothenburg, Sweden  
Email: {matts-ola.wessman, arne.svensson, erik.agrell}@s2.chalmers.se

**Abstract**—This paper investigates how convolutional and Reed–Solomon codes can be used to improve the performance of multiband-OFDM by utilizing the inherent frequency diversity of the new IEEE 802.15 UWB channel models.

A normalized amplitude autocovariance function of the Fourier transform of the channel impulse response is defined. Then the average coherence bandwidth of CM1, CM2, CM3, and CM4 are estimated to be 31.6, 16.3, 11.0, 5.8 MHz, respectively. Using the central limit theorem, we can expect that the performance of an uncoded OFDM system on CM1–CM4 without shadowing is the same as on a Rayleigh fading channel with uniformly distributed phase.

The performance of a convolutional code with rate 1/2 and constraint length 7 on CM2–CM4 without shadowing are up to 0.4 dB worse than that of on an uncorrelated Rayleigh fading channel. The loss for CM1 is around 1 dB. A block interleaver with 32 rows and 24 columns was used. This result is also valid for a convolutional code with rate 1/4 and constraint length 7.

For code rates around 2/3, the performance of a punctured convolutional code with soft-decision decoding is much better than that of the Reed–Solomon codes with with 6, 7, and 8 bits per symbol and hard-decision decoding.

## I. INTRODUCTION

In the near future, there will appear a demand for low cost, high-speed, wireless links for short range ( $< 10$  m) communication. Such links should support digital video transmission to be able to replace impractical cables. Ultra-wideband (UWB) systems with data rates of several hundred megabits per second could provide those features.

UWB systems can be divided into two groups: single band and multiband. Two commonly used single-band impulse radio systems are time-hopping spread-spectrum impulse radio (TH-UWB), [1], and direct-sequence spread-spectrum impulse radio (DS-UWB). Multiband-UWB and multiband-OFDM divide the spectrum into several bands, [2]–[5]. Multiband-OFDM was proposed for the physical layer within IEEE 802.15.3 that covers UWB communication in a wireless personal area network (WPAN).

Recently, IEEE proposed a channel model for UWB systems [6] based on the Saleh–Valenzuela model where multipath components arrive in clusters [7]. Before this channel model, the requirements from FCC [8] and the standardization within IEEE 802.15.3, the term ultra-wideband was mostly used for impulse radio. Lately, an increasing interest in achieving high data rates and using carrier-based system have been seen and the meaning of ultra-wideband has widened.

The IEEE UWB channel is constant during the transmission of one packet and no inherent time diversity is available within one packet. Fortunately, the channel is frequency selective which creates an opportunity to use error control coding to achieve frequency diversity.

The objective of this paper is to investigate the performance of convolutional codes and Reed–Solomon codes with the multiband-OFDM system on the IEEE UWB channel models and uncorrelated Rayleigh fading channels.

## II. SYSTEM MODEL

The system model consists of an outer encoder, an outer interleaver, an inner encoder, an inner interleaver, a multiband-OFDM modulator, a channel, a multiband-OFDM demodulator, an inner deinterleaver, an inner decoder, an outer deinterleaver, and a outer decoder.

### A. Error Control Coding and Interleaving

In this paper, only block interleavers were used where the encoded bits or symbols were written row-wise and read out column-wise. Two convolutional codes with optimum distance spectrum (ODS) that have rates 1/2 and 1/4 with constraint length  $v = 7$  are used [9]. The minimum free distance  $d_{\text{free}}$  of the codes are 10 and 20, respectively. The convolutional codes are denoted CC(2,1,7) and CC(4,1,7), respectively. Two punctured convolutional codes with rates 2/3 and 5/6 are used. They are obtained by puncturing the CC(2,1,7) code and are denoted PCC(3,2,7), and PCC(6,5,7), respectively. The puncturing matrixes employed are found in [10]. The  $d_{\text{free}}$  are 6 and 4 respectively. Soft-decision decoding assuming perfect channel knowledge was used in the Viterbi algorithm.

Reed–Solomon (RS) codes have burst error correcting capabilities and might thus be useful in our studied system. They use an alphabet of  $q$  symbols and usually  $q = 2^l$ .  $l$  bits are mapped to one of the  $q$  symbols. One code word consists of  $n_{\text{RS}} = q - 1 = 2^l - 1$  coded symbols and  $k_{\text{RS}} = n_{\text{RS}} - 2t$  information symbols. This code can correct  $t$  symbol errors. Three RS codes with  $l$  equal to 6, 7, and 8 bits per symbol having a rate around 2/3 are tested. A Reed–Solomon code is denoted RS( $n_{\text{RS}}, k_{\text{RS}}, l$ ) and for the investigated codes we have RS(63,41,6), RS(127,83,7), and RS(255,169,8), respectively. Those codes can correct 11, 22, and 43 symbol errors, respectively.

The errors in the output of a Viterbi decoder are always appearing in bursts due to the structure of the trellis of the code. The most probable length of a burst is equal to the constraint length  $v$ . High-rate block codes handles burst errors rather well. A concatenated scheme with an outer Reed–Solomon code and an inner convolutional code could improve the performance. If we set the number of bits in one RS symbol  $l$  to be larger than  $v$ , the error will most likely affect only one symbol. With this concatenated scheme, a symbol interleaver with  $n_{RS}$  rows and  $b$  columns could be used as the outer interleaver. This interleaver can cope with a burst length of  $b$  symbols. If we set  $l$  to be smaller than  $v$ , we can increase  $b$ .

### B. Multiband-OFDM

The multiband-OFDM system in [4] divides the spectrum  $B_{\text{tot}} = 1.584$  GHz into  $N_{\text{band}} = 3$  bands, each with a bandwidth of  $B = 528$  MHz. The OFDM symbol number  $o$  is then transmitted in band  $b$  given by  $b \equiv o \pmod{N_{\text{band}}}$ . Each OFDM symbol has  $N_{\text{st}} = 128$  subcarriers where the subcarrier bandwidth is  $B_s = B/N_{\text{st}} = 4.125$  MHz. One OFDM symbol has a duration of  $T_{\text{SYM}} = T_{\text{FFT}} + T_{\text{cp}} + T_{\text{GI}} = 312.5$  ns where  $T_{\text{FFT}} = 1/B_s = 242.4$  ns is the DFT integration time,  $T_{\text{cp}} = 60.6$  ns is the length of the cyclic prefix and  $T_{\text{GI}} = 9.5$  ns is the guard interval.  $N_{\text{SD}}$  is the number of data subcarriers per OFDM symbol. In total, there are  $N_{\text{band}}N_{\text{st}} = 384$  subcarriers in the 3 bands.

Under the assumptions of a long enough cyclic prefix, no doppler shift, linear hardware, and a constant channel during  $T_{\text{SYM}}$ , the subcarriers become independent. Then the received signal on subcarrier  $k$  can be modeled, with complex baseband representation, as

$$R_k = S_k G_k + n_k \quad 0 \leq k \leq N_{\text{band}}N_{\text{st}} - 1 \quad (1)$$

where  $S_k$  is a transmitted quadrature modulated symbol,  $n_k$  is complex valued white noise with variance  $N_0$  and  $G_k$  is a complex subcarrier channel gain. If  $g(t)$  is the channel impulse response,  $G_k = G(f_k)$  where  $G(f)$  is the continuous time Fourier transform of  $g(t)$  evaluated at subcarrier frequency  $f_k = f_0 + kB_s$ . Here  $f_0$  is set to 3.17 GHz. The values of  $k$  for band  $b = 0, 1, 2$  are  $[0, 127]$ ,  $[128, 255]$ , and  $[256, 378]$ , respectively.

The investigated receiver uses coherent detection assuming perfect channel estimates and QPSK modulation which gives

$$Y_k = R_k G_k^* = S_k |G_k|^2 + n_k G_k^* \quad 0 \leq k \leq N_{\text{band}}N_{\text{st}} - 1 \quad (2)$$

where  $*$  denotes complex conjugate.  $Y_k$  is used as a decision variable for hard-decision decoding. For soft-decision decoding, an optimum squared euclidean distance metric is calculated based on  $\{Y_k\}$ .

### C. Channel Models

The channel model of  $\{G_k\}$  in frequency domain used in (1) can be viewed as a time-frequency matrix with 378 rows. The number of columns is equal to the number of OFDM symbols per packet.

1) *IEEE UWB Channel Model*: The IEEE UWB channel model is a block fading channel where each of the gains  $\{G_k\}$  is constant during the whole packet. Moreover, channel realizations are independent between packets.

The IEEE UWB channel model is based on the Saleh–Valenzuela model where multipath components arrive in clusters [6], [7]. This multipath channel can be expressed as

$$h(t) = Xc(t) = X \sum_{l \geq 0} \sum_{k \geq 0} \alpha_{k,l} \delta(t - T_l - \tau_{k,l}) \quad (3)$$

where the real-valued multipath gain is defined by  $\alpha_{k,l}$  for cluster  $l$  and ray  $k$ . The  $l$ th cluster arrives at  $T_l$  and its  $k$ th ray arrives at  $\tau_{k,l}$  which is relative to the first path in cluster  $l$ , i.e.  $\tau_{0,l} = 0$ . The amplitude  $|\alpha_{k,l}|$  has a log-normal distribution and the phase  $\angle \alpha_{k,l}$  is chosen from  $\{0, \pi\}$  with equal probability. The expected value  $\mathbb{E}(|\alpha_{k,l}|^2)$  is proportional to  $\exp(-T_l/\Gamma - \tau_{k,l}/\gamma)$ , where  $\Gamma$  and  $\gamma$  denote a cluster- and a ray-decay factor, respectively. The interarrival time between two clusters  $T_{l+1} - T_l$  or two rays within one cluster  $\tau_{k+1,l} - \tau_{k,l}$  is exponentially distributed. Log-normal shadowing is modeled with  $X = 10^{n/20}$  where  $n$  has a normal distribution with mean  $\mu = 0$  and standard deviation  $\sigma_x = 3$ .

The continuous time Fourier transform of  $c(t)$  in (3) is

$$C(f) = \sum_{l \geq 0} \sum_{k \geq 0} \alpha_{k,l} e^{-j2\pi f(T_l + \tau_{k,l})}. \quad (4)$$

Note that in this article, the models are used with and without the shadowing term  $X$ . The channel gains of  $\{G_k\}$  from (1) are given by  $G_k = C(f_k)X$  and  $G_k = C(f_k)$  with and without shadowing, respectively. The shadowing will scale  $E_b$  with  $\mathbb{E}(|X|^2) = 10^{\sigma_x^2 \ln(10)/200 + \mu/10} \approx 1.27 \approx 1.04$  dB.

There are four different models, CM1, CM2, CM3 and CM4, for different channel characteristics. These are presented in Tab. I. In the rest of this paper, IEEE UWB models without shadowing are denoted CM1, CM2, CM3, and CM4, while models with shadowing are referred to as CM1X, CM2X, CM3X, and CM4X.

TABLE I  
THE IEEE UWB CHANNEL MODEL

Model Characteristic	CM1	CM2	CM3	CM4	unit
Tx Rx separation	0-4	0-4	4-10		m
(Non-)line of sight	LOS	NLOS	NLOS	NLOS	

2) *Uncorrelated Rayleigh Fading Channel*: The purpose of using an uncorrelated Rayleigh fading channel is to see how much the coherence bandwidth and the lack of time diversity of the IEEE UWB channels degrade the performance. The uncorrelated Rayleigh fading channel sets the  $\{G_k\}$  in the time-frequency matrix to have uncorrelated Rayleigh fading amplitudes and uniformly distributed phases.

## III. SYSTEM PARAMETERS AND ASSUMPTIONS

In this paper, we use, for simplicity,  $N_{\text{SD}} = 128$  of the 128 carriers per OFDM symbol for data, although only 100 are

used in the multiband-OFDM system in [4]. The convolutional code is used with a bit interleaver with 32 rows and 24 columns. The length of the interleaver is 768 which the number of bits in three OFDM symbols with QPSK.

$E_b/N_0$  is defined as  $\mathbb{E}(|S_k G_k|^2) / (\mathbb{E}(|n_k|^2) R_c \log_2 M)$  where  $R_c$  is the channel code rate and  $M$  is the alphabet size. This definition do not consider the energy loss due to pilots and cyclic prefix.

The simulations of the multiband-OFDM system was performed using complex baseband representation in the frequency domain as given by (1). The synchronization is assumed to be perfect and the effects of the antenna and other nonlinear hardware have been neglected.

#### IV. ANALYSIS

##### A. Analysis of IEEE UWB Channel Model

The normalized amplitude autocovariance of  $C(f)$  in (4) is defined as

$$\rho_a(v) = \text{Cov}(|C(f)|, |C(f+v)|) / \text{Var}(|C(f)|). \quad (5)$$

The coherence bandwidth  $B_c$  is defined here via  $\rho_a(B_c) = 0.5$ . The mean excess delay  $\bar{\tau}^{(i)}$ , the RMS delay spread  $\sigma_\tau^{(i)}$ , and  $B_c^{(i)}$  were calculated for one realization  $i$  of  $c^{(i)}(t)$  in (3). Then the average of  $\bar{\tau}^{(i)}$ ,  $\sigma_\tau^{(i)}$ , and  $B_c^{(i)}$  denoted  $\bar{\tau}$ ,  $\bar{\sigma}_\tau$ , and  $\bar{B}_c$  were numerically estimated from a large number of realizations  $\{c^{(i)}(t)\}$ . The standard deviation of those random variables were also estimated. Tab. II contains the estimated values. The scaling factor  $q = 1/\bar{\sigma}_\tau \bar{B}_c$  gives the relationship between the coherence bandwidth and the RMS delay spread. The values of  $q$  is between 6 and 7.3 which is close to the normal rule of thumb that uses  $2\pi$ . By dividing the average coherence bandwidth with the subcarrier bandwidth  $B_s = 4.125 \cdot 10^6$  Hz, the average number of correlated subcarriers,  $\bar{k}$ , is obtained.

TABLE II  
ESTIMATED MODEL CHARACTERISTICS OF CM1 TO CM4

Estimated Characteristic	CM1	CM2	CM3	CM4	unit
Avg. mean excess delay $\bar{\tau}$	4.85	9.57	15.58	28.47	ns
Standard deviation of $\{\bar{\tau}^{(i)}\}$	1.45	2.10	5.48	8.51	ns
Avg. RMS delay spread $\bar{\sigma}_\tau$	5.30	8.40	14.39	25.91	ns
Standard deviation of $\{\sigma_\tau^{(i)}\}$	1.31	0.99	3.33	5.58	ns
Avg. coherence bandw. $\bar{B}_c$	31.60	16.25	11.03	5.79	MHz
Standard deviation of $\{B_c^{(i)}\}$	10.97	3.46	3.95	2.12	MHz
$q = 1/\bar{\sigma}_\tau \bar{B}_c$	5.97	7.33	6.30	6.67	
$\bar{k} = \bar{B}_c/4.125$ MHz	7.7	3.9	2.7	1.4	

When the number of taps is large, the central limit theorem tells us that  $C(f)$  in (4) will converge in distribution to  $I + jQ$  where  $I$  and  $Q$  are normally distributed random variables with zero mean and variance  $\sigma^2$ . The zero mean is due to the fact that  $\mathbb{E}(\alpha_{k,l}) = 0$ . Consequently, we expect that the performance of an uncoded OFDM system on CM1–CM4 and on a Rayleigh fading channel with uniformly distributed phase are the same.

The amplitude of the Fourier transform  $|H(f)| = X|C(f)|$  has a Suzuki distribution [11] for each  $f$  since  $X$  is log-normally distributed. We have numerically verified, with high accuracy, that the estimated pdfs of the amplitude  $|C(f)|$  and the phase  $\angle C(f)$  are Rayleigh and uniformly distributed, respectively.

##### B. Analysis of Size of Block Interleaver

When designing the block interleaver, we have to consider both  $\bar{k}$  and the fact that the standard deviation of  $\{B_c^{(i)}\}$  is roughly one third of  $\bar{B}_c$ . The number of columns have to be several times larger  $\bar{k} \log_2 M$ . For the convolutional code, one rule of thumb is that the number of rows has to be larger than  $5(v-1)$  so that influence of the fading dips on the Viterbi algorithm are almost negligible.

##### C. Performance Analysis of Convolutional Codes

The union bound of the bit error rate of a convolutional code is given by [12, p. 488]

$$P_b(E_b/N_0) < \frac{1}{k_{CC}} \sum_{d=d_{\text{free}}}^{\infty} c_d P_2(d, E_b/N_0) \quad (6)$$

where  $c_d$  is the distance spectrum defined as the total number of information bit errors for all error events of length  $d$ . The distance spectrum for the ODS convolutional codes used in this paper is found in [9].  $P_2(d, E_b/N_0)$  is the pairwise error probability that a correct path and an incorrect path differ in  $d$  positions. (6) is also valid for punctured convolutional codes and the distance spectrum for several punctured codes can be found in [10].

Now we assume that we have coherent detection with perfect channel estimates on a perfectly interleaved Rayleigh fading channel and a soft-decision Viterbi decoder. With  $R_c$  as the code rate, the pairwise error probability becomes [12, p. 859]

$$P_2(d, E_b/N_0) = p^d \sum_{l=0}^{d-1} \binom{d-1+l}{l} (1-p)^l \quad (7)$$

with

$$p = \frac{1}{2} \left( 1 - \sqrt{\frac{R_c E_b/N_0}{1 + R_c E_b/N_0}} \right) \quad (8)$$

When the outer code is Reed–Solomon and the inner code is convolutional, the knowledge of the symbol error probability,  $P_s$ , at the output of the Viterbi decoder is valuable. One symbol is defined as a Reed–Solomon code symbol of  $l$  bits. A simple upper bound on  $P_s$  is

$$P_s \leq l P_b \quad (9)$$

A better upper bound, which is only valid for  $k_{CC} = 1$ , considers the transfer function  $T(D, N, J)$  of the convolutional code with constraint length  $v$  and is given by [13]

$$P_s < \sum_{d=d_{\text{free}}}^{\infty} f_d P_2(d, \gamma_b) \quad (10)$$

with  $f_d$  as the polynomial coefficients in

$$\sum_{d=d_{\text{free}}}^{\infty} f_d D^d = (l-v)T(D, 1, 1) + \left. \frac{\partial T(D, N, J)}{\partial J} \right|_{N=1, J=1} \quad (11)$$

where we recognize  $T(D, 1, 1) = \sum_{d=d_{\text{free}}}^{\infty} a_d D^d$  and  $a_d$  as the number of incorrect paths of Hamming weight  $d$ . Note that the differentiation is with respect to  $J$ . The exponent of  $J$  gives the length of the path that merges with the all-zero path for the first time.

#### D. Performance Analysis of Reed–Solomon Codes

The probability of a code word error,  $P_W$ , for a Reed–Solomon code that can correct  $t$  symbols on a channel with uncorrelated symbol errors and a symbol error probability  $P_s$  is given by

$$P_W = 1 - \sum_{j=0}^t \binom{n_{\text{RS}}}{j} P_s^j (1 - P_s)^{n_{\text{RS}}-j} \quad (12)$$

For 6, 7, and 8 bits per symbol, one RS-symbol is transmitted on 3, 3.5 and 4 subcarriers, respectively, when QPSK is used. Also, the length of one code word is 378, 889, 2040 bits, respectively. With 8 bits per symbol, one code word is transmitted on almost 8 OFDM symbols. Thus, the first third and the second third of one code word will be affected by the same subcarrier channel gains  $\{G_k\}$ .

#### E. Performance Analysis of Concatenated Codes

When the outer code is a Reed–Solomon code and the inner code is a convolutional code, the word error rate can be upper bounded by substituting  $P_s$  from (9) or (10) in (12). The performance of this RS+CC code is improved if a symbol interleaver is used between the Viterbi decoder and the RS decoder.

#### F. Diversity Order

On an uncorrelated Rayleigh fading channel, it can be shown [14] that the average bit error rate,  $\bar{P}_b$ , approaches  $K/(E_b/N_0)^D$  when  $E_b/N_0$  approaches infinity. This defines the diversity order  $D$ . Since the bit error rate is proportional to the word error rate, (12) shows that  $D = t + 1$  for a block code with hard decoding that corrects  $t$  errors. For convolutional codes with soft decoding,  $D$  equals  $d_{\text{free}}$  which can be seen from (6). Further, the concatenated Reed–Solomon and convolutional code scheme will get a diversity order of  $d_{\text{free}}(t + 1)$ .

### V. NUMERICAL RESULTS

For each channel model and  $E_b/N_0$ , at least 500 channels were used in the presented results. Only QPSK modulation was used in all numerical simulations.

For all the convolutional codes, a block interleaver with 32 rows and 24 columns was used. In Fig. 1, we see that the uncoded system on CM1 and CM4 has the same performance

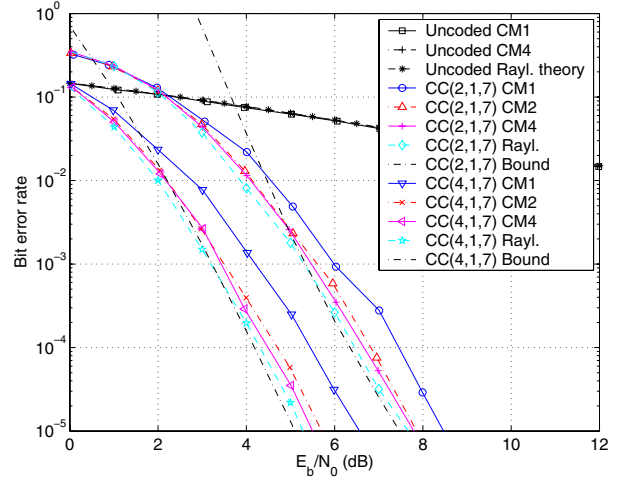


Fig. 1. The bit error rate with convolutional codes (2,1,7) and (4,1,7) on channel models CM1–CM4 and on an uncorrelated Rayleigh fading channel. Also the uncoded system and the union bound for convolutional codes are shown.

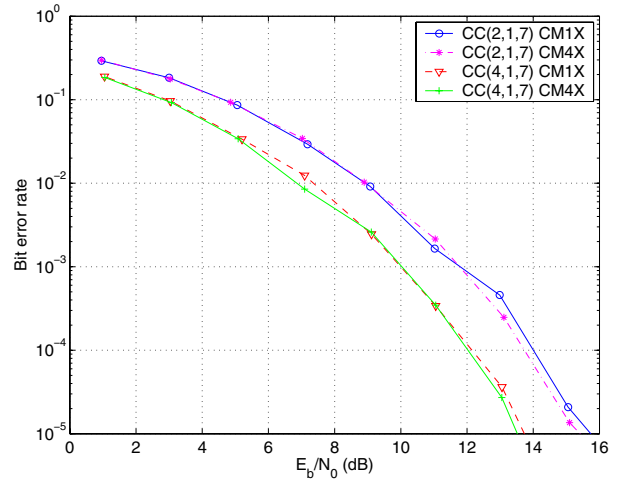


Fig. 2. The bit error rate of the with convolutional codes (2,1,7) and (4,1,7) on channel models CM1X and CM4X with shadowing

as that on a flat Rayleigh fading, which agrees with our previous conclusion that the subcarrier channel gains,  $\{|C(f)|\}$ , have Rayleigh distributed amplitudes. Fig. 1 also shows the bit error rate when the convolutional codes with a constraint length of 7 and code rate equal to 1/2 and 1/4 on the channel models CM1, CM2, and CM4 and on an uncorrelated Rayleigh fading channel. The bound from (6) for the convolutional codes is also plotted. The performance on CM2–CM4 without shadowing are up to 0.4 dB worse than on an uncorrelated Rayleigh fading channel. The loss for CM1 is around 1 dB at bit error rates below  $10^{-4}$ .

Fig. 2 shows the bit error rates for CC(2,1,7) and CC(4,1,7) on CM1X and CM4X with shadowing. For each code, the performance on CM1X and CM4X is almost the same. Compare this indication with the difference for the same codes on CM1 and CM4 in Fig. 1.

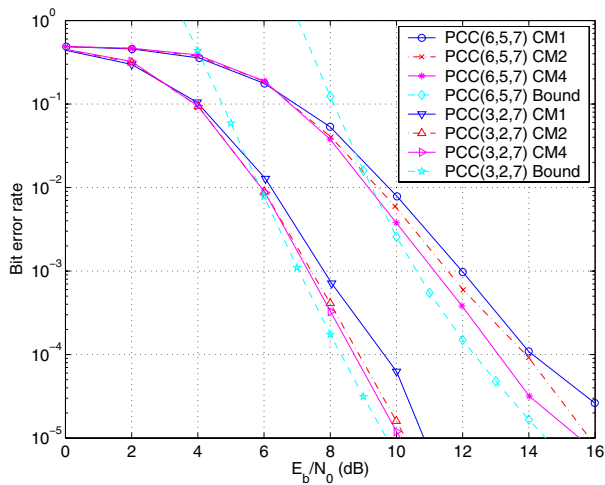


Fig. 3. The bit error rate of the punctured convolutional codes with rate  $2/3$  and  $5/6$  and constraint length 7 on CM1, CM2, and CM4 without shadowing.

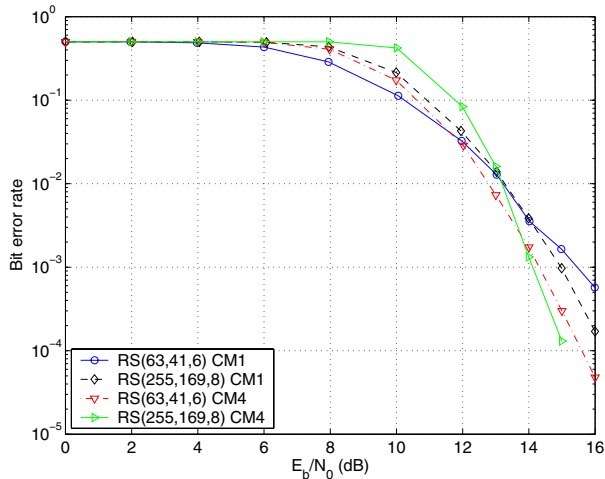


Fig. 4. The bit error rate of Reed-Solomon codes with 6, 7 and 8 bits per symbol and rates around  $2/3$  on CM1 and CM4 without shadowing.

The bit error rates for the punctured convolutional codes PCC(3,2,7) and PCC(6,5,7) on CM1, CM2, and CM4 without shadowing are shown in Fig. 3 with the union bound in (6). Still the performance on CM1 is worse than CM2 and the performance on CM2 is worse than on CM4.

The performance of Reed-Solomon codes without any interleaver with  $l$  equal to 6, 7 and 8 bits per symbol with a rate around  $2/3$  was investigated using QPSK and hard-decision decoding. As seen in Fig. 4, the performance is almost the same for 6 and 8 bits per symbol that have 378 and 2040 coded bits per codeword. It seems that the performance on CM4 is better than on CM1. This is also valid for 7 bits per symbol that is not shown here. Clearly, the performance of the punctured convolutional code with rate  $2/3$  is much better than those Reed-Solomon codes.

## VI. CONCLUSIONS

The following conclusions are drawn from this study:

- The average coherence bandwidth of CM1, CM2, CM3, and CM4 are 31.6, 16.3, 11.0, 5.8 MHz, respectively. The average number of correlated subcarriers are 7.7, 3.9, 2.7, and 1.4 for CM1–CM4, respectively.
- Using the central limit theorem, we can expect that the performance of an uncoded OFDM system on CM1–CM4 and on a Rayleigh fading channel with uniformly distributed phase are the same.
- The performance of convolutional codes with rate  $1/2$  and a constraint length of 7 is almost the same on CM2–CM4 and on an uncorrelated Rayleigh fading channel when using a block interleaver with 32 rows and 24 columns. For the same code, the difference on CM1 and CM4 that could be seen without shadowing is not visible when shadowing is applied. Those two conclusions are also valid for the rate  $1/4$  code with constraint length 7.
- For code rates around  $2/3$ , the performance of the punctured convolutional code with soft-decision decoding is much better than the Reed-Solomon codes with hard-decision decoding.

## ACKNOWLEDGMENT

The authors would like to acknowledge the contribution by Rana Chebl and Vittorio Fougatsaro. This work has been funded by the Swedish Research Council and PCC++.

## REFERENCES

- [1] M. Z. Win and R. A. Scholtz, "Ultra-wide bandwidth time-hopping spread-spectrum impulse radio for wireless multiple-access communications," *IEEE Trans. Commun.*, vol. 48, pp. 679–689, Apr. 2000.
- [2] M. Pendergrass, "Time Domain supporting text for 802.15.3 alternate physical layer proposal", IEEE P802.15-03/144r1, IEEE P802.15 Working Group for Wireless Personal Area Networks, Mar. 2003.
- [3] G. Shor, "TG3a-Wisair-CFP-Presentation", IEEE P802.15-03/151r3, IEEE P802.15 Working Group for Wireless Personal Area Networks, May 2003.
- [4] "Multi-band OFDM Physical Layer Proposal for IEEE 802.15 Task Group 3a", www.multibandofdm.org.
- [5] R. Chebl and V. G. Fougatsaro "Performance of multiband-OFDM in IEEE UWB channel models," *M.Sc. thesis report*, Signals and Systems, Chalmers Univ. of Technology, Sweden, 2004.
- [6] J. Foerster et al., "Channel modeling sub-committee report final," *IEEE P802.15 Wireless Personal Area Networks, P802.15-02/490r1-SG3a*, Feb. 2003.
- [7] A. Saleh and R. Valenzuela, "A statistical model for indoor multipath propagation," *IEEE Journal on Select. Areas Commun.*, vol. 5, pp. 128–137, Feb. 1987.
- [8] "Revision of part 15 of the commission's rules regarding ultra-wideband transmission systems," Federal Communications Commission, First Report and Order, ET Docket 98–153, Apr. 2002.
- [9] P. Frenger, P. Orten, and T. Ottosson, "Convolutional codes with optimum distance spectrum," *IEEE Commun. Lett.*, vol. 3, pp. 317–319, Nov. 1999.
- [10] D. Haccoun and G. Begin, "High-rate punctured convolutional codes for Viterbi and sequential decoding" *IEEE Trans. on Comm.*, Vol. 37, pp. 1113–1125, Nov. 1989.
- [11] Suzuki, H. "A Statistical Model for Urban Radio Propagation" *IEEE Trans on Comm.*, vol. 25, no. 7, pp. 673–680, July 1977
- [12] J. G. Proakis, *Digital communications*, McGraw-Hill, 4th ed., 2001.
- [13] R. D. Cideciyan, E. Eleftheriou, and M. Rupp, "Concatenated Reed-Solomon/convolutional coding for data transmission in CDMA-based cellular systems," *IEEE Trans. Commun.*, vol. 45, pp. 1291–1303, Oct. 1997.
- [14] J. B. Anderson and A. Svensson, *Coded Modulation Systems*, Kluwer Academic/ Plenum Publisher, 2003.